

# Understanding the low-frequency modes in disordered systems at single-particle level

Peng Tan<sup>1</sup>, Ning Xu<sup>2</sup>, Andrew B. Schofield<sup>3</sup>, and Lei Xu<sup>1</sup>

<sup>1</sup>*Department of Physics, The Chinese University of Hong Kong, Hong Kong, China*

<sup>2</sup>*Department of Physics, University of Science and Technology of China, Hefei, China*

<sup>3</sup> *The School of Physics and Astronomy,  
University of Edinburgh, Edinburgh, UK*

(Dated: June 16, 2018)

**Normal modes provide a fundamental basis for understanding crucial properties of solids, such as the thermal conductivity, the heat capacity and the sound propagation[1–3]. While the normal modes are excellently described by plane waves in crystals, they are far less understood in disordered systems, due to the great difficulties in characterizing the heterogeneous vibrational behaviors. Using charged colloids with long-range repulsion, we successfully make different disordered systems without any contact friction, whose normal modes can be visualized at single-particle level. In these systems, we directly tackle the long-time outstanding puzzle in condensed matter physics: the microscopic origin of the low-frequency modes in disordered systems. For the first time, we experimentally clarify that the low-frequency modes are caused by the collective resonance of relatively disordered particles (or soft structures) coupled with long-wavelength transverse excitations, settling this puzzle at single-particle level. Next to these low-frequency modes in the density of states, we also observe a plateau due to isostaticity, verifying the fundamental prediction of jamming model [4–6]. Moreover, we reveal the intrinsic correlation between the low-frequency modes and the real dynamics, which may lead to a universal mechanism for aging, melting and yielding.**

One important unsolved problem in condensed matter physics is to understand the normal modes of disordered systems. Unlike crystals, whose particles have identical surroundings and vibrate as plane waves, the particles of disordered systems have different local environment and oscillate distinctively. To fully understand their vibrations, therefore, we must correlate individual particles' motions with their local environment, most ideally at single-particle level. Because of experimental difficulties, however, such studies are rare, leaving important questions unsolved. In particular, disordered systems have much more low-frequency modes than crystals, which often form a broad boson peak in the  $D(\omega)/\omega^{d-1}$  spectrum. These low-frequency modes are generally believed to cause the anomalous properties in heat capacity, thermal conductivity and acoustic behaviors. The origin and properties of these modes are still open to debate. A number of models have been proposed. In the energy landscape model, the excess low-frequency modes are explained as the signature from a minima-dominated phase to a saddle-point-dominated phase[7]. In the jamming model, the jamming transition at zero temperature (point J) is found responsible: it produces a plateau in  $D(\omega)$  as the result of isostaticity, and creates extra modes at low frequencies [4–6, 8–13]. Detailed numerical analysis of the low-frequency modes suggests their possible origin as transverse phonons associated with defective soft structures[14]. Experimentally, Raman, X-ray, and neutron scatterings are commonly used to measure the normal mode spec-

trum. It is shown that the low-frequency modes have collective character[15] and non-acoustic properties[16]. Most recently, the experiments in colloidal systems begin to examine the normal modes at single-particle level[17–20]. Despite extensive studies, however, the microscopic origin of the low-frequency modes has never been experimentally clarified, which is the main focus of this study.

We suspend PMMA particles of diameter  $a = 2.0\mu m$  (polydispersity  $< 3\%$ ) in density and refractive-index matched solvent, between two glass substrates (Methods). In the weakly polar solvent, the particles and the walls carry the same type of charges and interact with long-range repulsion [21, 22]. Since there is no particle-particle and particle-wall contact, we completely eliminate the contact frictions in our system. Using confocal microscopy, we track every particle’s motion with excellent spatial( $15nm$ ) and temporal ( $30s^{-1}$ ) resolutions. We study perfect 2D samples by one single particle layer between two glass substrates. To quantitatively describe individual particle’s local environment, we directly measure each particle’s local orientational order parameter,  $\Psi_{6i}$ , determined by the nearest neighbors’ arrangement:  $\Psi_{6i} = 1$  means perfect hexagonal arrangement around particle  $i$  and  $\Psi_{6i} = 0$  indicates totally random arrangement(see Methods for exact definition). We use different colors to represent the different  $\Psi_{6i}$  values in Fig.1a. Clearly our heterogeneous samples contain both ordered and disordered particles, with  $\Psi_{6i}$  ranging from 0 to 1. We can also systematically vary the overall amount of disorder: by increasing the number density, we increase the particle interaction and achieve more ordered samples, as shown by sample-A through sample-D in Fig.1a and Fig.1b.

For each sample, we track the motions of all particles for 2000 frames and extract the normal modes with covariance matrix method[18–20](Methods). This method is valid for stable and metastable systems, in which no particle should rearrange; we therefore check every frame to make sure no particle rearranges for the entire process. Within the measurement time, every particle moves around its well-defined equilibrium position and the system is metastable; while for longer time, thermal motions cause rearrangements and the system relaxes. This relaxation limits our measurement time to 2000 frames. To compare the behaviors of particles under different local environment, in each sample we divide all particles into two groups: the relatively disordered particles with  $\Psi_{6i}$  less than the system average ( $\Psi_{6i} < \overline{\Psi_{6i}}$ ), and the relatively ordered particles with  $\Psi_{6i}$  larger than the system average ( $\Psi_{6i} > \overline{\Psi_{6i}}$ ). The comparison between the two groups will clarify the special role of the disordered particles in the low-frequency modes. Fig.1c shows the mean square displacement(MSD) for the relatively disordered particles (labeled as “dis”) and

the relatively ordered particles (labeled as “ord”) in samples A and C. The disordered curves are higher than the corresponding ordered ones, indicating the qualitatively larger movements of the disordered particles. In addition, all curves are below the dashed line of free diffusion, as the result of caging effect.

From the particle tracking, we extract the normal modes at single-particle level, over three orders of magnitude in frequency. We plot the density of states,  $D(\omega)$ , in Fig.2a [23]. For each curve, we can clearly identify two characteristic frequencies,  $\omega^\dagger$  and  $\omega^\ddagger$ , which divide  $D(\omega)$  into three regimes: a rapidly rising low-frequency regime ( $\omega < \omega^\dagger$ ), a medium-frequency plateau ( $\omega^\dagger < \omega < \omega^\ddagger$ ), and a high-frequency regime ( $\omega > \omega^\ddagger$ ). For the first time, we experimentally measure a plateau in  $D(\omega)$ , which is predicted in the jamming model as the result of isostaticity [4, 5, 11]. This plateau did not appear in previous measurements[18–20], possibly due to the effect of contact frictions[24]. From A to D, as system disorder decreases, the number of the low-frequency modes reduces, the plateau width between  $\omega^\dagger$  and  $\omega^\ddagger$  shrinks, and the plateau height lowers. The diminishing of the plateau should come from the reduced amount of isostatic particles. Fig.2b plots the  $D(\omega)/\omega^{d-1}$  spectrum and shows the boson peak in samples C, D but not in A, B. This is again consistent with the jamming model: the boson peak shifts to lower frequencies in less compressed systems such as A, B[4, 5, 11].

To illustrate the microscopic origin of the low-frequency modes, we analyze the normal modes at single-particle level. Fig.3a shows three typical modes in the three different regimes of sample A (see Supplementary Information for other samples). The low-frequency mode is quasi-localized with large-scale collective correlations, consistent with the jamming model[4, 6, 11, 13]; while the other two modes look rather random. Further inspection on the low-frequency mode reveals that its large-amplitude vibrations mostly occur at the disordered particle sites. To quantitatively verify this, we compute the average squared amplitude of the relatively disordered particles,  $\overline{A^2}_{dis}$ , and the relatively ordered particle,  $\overline{A^2}_{ord}$ . Their ratio,  $\overline{A^2}_{dis}/\overline{A^2}_{ord}$ , quantifies the relative vibrational strength between the two groups. We plot this ratio at all frequencies in Fig.3c. In all the samples,  $\overline{A^2}_{dis}/\overline{A^2}_{ord}$  is greater than one at small  $\omega$  but quickly drops to unity as  $\omega$  increases. This quantitatively proves that the disordered particles vibrate stronger than the ordered ones at low frequencies. Moreover, the transition frequency, where  $\overline{A^2}_{dis}/\overline{A^2}_{ord}$  approaches unity, can separately define an  $\omega^\dagger$ , which coincides exactly with the one found in  $D(\omega)$  (Fig.2a). These data strongly suggest that all the low-frequency modes in the first regime ( $\omega < \omega^\dagger$ ) are caused by the large-amplitude resonance of disordered particles, clarifying the microscopic origin of the low-frequency modes.

While the polarization vectors in real space reveal the resonance, their Fourier transform in  $q$  space brings further insights. In Fig.3b, we decompose the same modes of Fig.3a into transverse and longitudinal Fourier components (see Methods), and show their  $q$  space distribution within the first Brillouin zone  $[-\frac{\pi}{\sigma} < q_x, q_y < \frac{\pi}{\sigma}]$  ( $\sigma$  is the typical distance between two neighboring particles). We focus on the low-frequency mode in column one ( $\omega \ll \omega^\dagger$ ): the transverse component has much larger overall magnitude and dominates the longitudinal one, verifying the transverse nature of the low-frequency modes [14]. Moreover, it mostly concentrates on small  $q$  values, indicating long-wavelength transverse excitations. At the medium frequency ( $\omega^\dagger < \omega < \omega^\ddagger$ ), the transverse component becomes uniformly distributed. When the high frequency is reached ( $\omega \gg \omega^\ddagger$ ), the magnitude at small  $q$  decreases sharply, making the center more “black” than the edge. The longitudinal component keeps spreading throughout  $q$  space as  $\omega$  increases.

To illustrate the overall evolution of the transverse and longitudinal components, we plot their average magnitude at all frequencies in Fig.3d. For low and medium frequencies, the transverse curves dominate the longitudinal ones, consistent with Fig.3b. More interestingly, each transverse curve also contains two characteristic frequencies,  $\omega^\dagger$  and  $\omega^\ddagger$ , that coincide with the ones found in  $D(\omega)$ . The wonderful agreement of  $\omega^\dagger$  and  $\omega^\ddagger$  determined by various approaches is demonstrated in Fig.3e, which summarizes different properties of the normal modes from different aspects. Combining all the properties of the first regime ( $\omega < \omega^\dagger$ ), we now draw the final conclusion on the low-frequency modes: *they are caused by the collective resonance of the relatively disordered particles, coupled with long-wavelength transverse excitations*. This conclusion is based on the direct measurements of every particle’s local environment and vibrational properties in real and Fourier space, and may also apply to other disordered systems.

Besides the microscopic origin, we illustrate another interesting property of the low-frequency modes: their ability to drive the real dynamics[25, 26]. By projecting the long-time (2000 frames) displacement field onto the normal mode basis (Methods)[27], we find the displacement mainly falls on the low-frequency modes. Fig.4a and 4b compare the displacement field and the superposition of ten most contributed low-frequency modes in sample A, both vector fields look quite similar. Their difference is shown in Fig.4c: the small residue proves their excellent agreement unambiguously. Fig.4d shows the sum of the projection probabilities,  $|c_\omega|^2$ , and quantitatively confirms the major contributions from the low-frequency modes. The fact that we can wonderfully map the complex displacements of thousands of particles with only ten low-frequency modes is rather astonishing. It demonstrates that although the real dynamics is thermally driven, it is not

random during a long-time interval; instead it follows specific low-frequency modes. Similarly, we suspect that aging, melting and yielding may also be initiated by specific low-frequency modes, and speculate the excitation of these modes as the universal mechanism for these general phenomena.

In this study, we experimentally illustrate the origin and properties of the low-frequency modes in disordered systems. By dividing all particles into different groups with respect to their local environment ( $\Psi_{6i}$ ), we explicitly demonstrate the important role of the relatively disordered particles. We note that  $\Psi_{6i}$  is just one of the many parameters that can be used. For example, grouping particles according to their fluctuations around equilibrium positions (local Debye-Waller factor) can yield similar results (Supplementary Information). Therefore, our grouping approach can be generalized and applied to many other disordered systems, thus providing a general method to analyze heterogeneous systems [28–30].

## Methods

**Sample Preparation.** The PMMA particles are dyed with NBD and grafted with Polyhydroxysebacic acid (PHSA) polymers. They are suspended in the mixture of Iododecane and Iodododecane (volume ratio 1:4), forming density and refractive-index matched systems. The PHSA polymers are slightly charged in the solvent, yielding the long-range repulsive potential between particles. We make 2D samples by trapping one layer of particles between two cover glasses. The glass surfaces are also grafted with PHSA polymers, and repel the particles from large distance.

**Local Orientational Order Parameter.** The local orientational order parameter for particle  $i$  is defined as:  $\Psi_{6i} = \frac{1}{n_i} \left| \sum_{m=1}^{n_i} e^{j6\theta_{mi}} \right|$ . Here  $n_i$  is the number of nearest neighbors of particle  $i$ , and  $\theta_{mi}$  is the angle between  $\mathbf{r}_m - \mathbf{r}_i$  and the x axis.  $\Psi_{6i} = 1$  means the perfect hexagonal arrangement of six nearest neighbors and  $\Psi_{6i} = 0$  means totally random arrangement.

**Covariance Matrix Method.** From particle tracking, we can construct the covariance matrix and solve for the normal modes. The elements of the covariance matrix are defined as:

$$C_{i,j} = \langle (\mathbf{u}_i(t) - \langle \mathbf{u}_i(t) \rangle) (\mathbf{u}_j(t) - \langle \mathbf{u}_j(t) \rangle) \rangle \quad (1)$$

where  $\mathbf{u}(t)$  is the particle displacement at time  $t$ , and  $i, j = 1, \dots, 2N$  run over the  $N$  particles and their x and y coordinates.  $\langle \rangle$  means time average. Diagonalizing the matrix yields eigenvectors and eigenvalues. Since the covariance matrix and the dynamic matrix have the relationship:  $D_{i,j} = \frac{k_B T}{m} (C^{-1})_{i,j}$ , the covariance matrix eigenvectors give the polarization vectors of the normal modes, and the covariance matrix eigenvalues,  $\lambda = \frac{k_B T/m}{\omega^2}$ , yield the angular frequencies  $\omega$ .

**Transverse and Longitudinal Components.** The transverse and longitudinal components of the normal modes in Fourier space are defined as:

$$f_{\omega,tr}(\mathbf{q}) = |\sum_i(\hat{\mathbf{q}} \times \mathbf{e}_{i,\omega})\exp(i\mathbf{q} \cdot \mathbf{r}_i)|^2 - \text{transverse} \quad (2)$$

$$f_{\omega,lo}(\mathbf{q}) = |\sum_i(\hat{\mathbf{q}} \cdot \mathbf{e}_{i,\omega})\exp(i\mathbf{q} \cdot \mathbf{r}_i)|^2 - \text{longitudinal} \quad (3)$$

Here  $\omega$  labels the mode.  $\mathbf{e}_i$  and  $\mathbf{r}_i$  are the polarization vector and the equilibrium position vector of particle  $i$ . The summation is over all particles.

**Projection of the Real Dynamics onto the Normal Modes.** We first obtain the displacement field during the time window of  $\tau=2000$  frames:

$$|\delta r(\tau)\rangle = |\delta r(t_0 + \tau)\rangle - |\delta r(t_0)\rangle \quad (4)$$

We then project it onto the normal mode  $|\omega\rangle$ , with the prefactor  $c_\omega$  determined by:

$$c_\omega = \frac{\langle \omega | \delta r(\tau) \rangle}{\sqrt{\langle \delta r(\tau) | \delta r(\tau) \rangle}} \quad (5)$$

The prefactors satisfy  $\sum |c_\omega|^2 = 1$  for a complete set of modes. We find that for some specific low-frequency modes, the  $|c_\omega|^2$  values are particularly large. These modes can therefore be regarded as the driving modes of the real dynamics.

- 
- [1] Phillips, W.A.(ed.) *Amorphous Solids: Low Temperature Properties* (springer, 1981).
  - [2] Angell, C. A. Formation of glasses from liquids and biopolymers. *Science* **267**, 633-636 (1995).
  - [3] Frick, B. & Richter, D. The microscopic basis of the glass transition in polymers from neutron scattering studies. *Science* **267**, 1939-1945 (1995).
  - [4] Silbert, L. E. Liu, A. J. & Nagel, S. R. Vibrations and diverging length scales near the unjamming transition. *Phys. Rev. Lett.* **95**, 098301 (2005).
  - [5] Wyart, M., Nagel, S. R. & Witten, T. A. Geometric origin of excess low-frequency vibrational modes in weakly connected amorphous solids. *Europhys. Lett.* **72**, 486-492(2005).
  - [6] Silbert, L. E., Liu, A. J. & Nagel, S. R. Normal modes in model jammed systems in three dimensions. *Phys. Rev. E* **79**, 021308 (2009).
  - [7] Grigera, T., Martn-Mayor, V., Parisi, G. & Verrocchio, P. Phonon interpretation of the boson peak in supercooled liquids. *Nature* **422**, 289-292 (2003).

- [8] Grest, G. S., Nagel, S. R. & Rahman, A. Longitudinal and transverse excitations in a glass. *Phys. Rev. Lett.* **49**, 1271 (1982).
- [9] Liu, A. J. & Nagel, S. R. Jamming is not just cool any more. *Nature* **396**, 21-22 (1998).
- [10] O'Hern, C. S., Langer, S. A., Liu, A. J. & Nagel, S. R. Random packings of frictionless particles. *Phys. Rev. Lett.* **88**, 075507 (2002).
- [11] Wyart, M., Silbert, L. E., Nagel, S. R. & Witten, T. A. Effects of compression on the vibrational modes of marginally jammed solids. *Phys. Rev. E* **72**, 051306 (2005).
- [12] Xu, N., Vitelli, V., Wyart, M., Liu, A. J. & Nagel, S. R. Energy transport in jammed sphere packings. *Phys. Rev. Lett.* **102**, 038001 (2009).
- [13] Xu, N., Vitelli, V., Liu, A. J. & Nagel, S. R. Anharmonicity and quasi-localization of the excess low-frequency vibrations in jammed solids-Modes for mechanical failure. *Europhys. Lett.* **90**, 56001 (2010).
- [14] Shintani, H. & Tanaka, H. Universal link between the boson peak and transverse phonons in glass. *Nat. Mater.* **7**, 870 (2008).
- [15] Chumakov, A. I. *et al.* Collective nature of the boson peak and universal transboson dynamics of glasses. *Phys. Rev. Lett.* **92**, 245508 (2004).
- [16] Rufflé, B., Parshin, D. A., Courtens, E. & Vacher, R. Boson peak and its relation to acoustic attenuation in glasses. *Phys. Rev. Lett.* **100**, 015501 (2008)
- [17] Zhang, Z., *et al.* Thermal vestige of the zero-temperature jamming transition. *Nature* **459**, 230-233 (2009).
- [18] Ghosh, A., *et al.* Density of states of colloidal glasses, *Phys. Rev. Lett.* **104**, 248305 (2009).
- [19] Chen, K. *et al.* Low-frequency vibrations of soft colloidal glasses. *Phys. Rev. Lett.* **105**, 025501 (2010).
- [20] Kaya, D., Green, N. L., Maloney, C. E. & Islam, M. F. Normal modes and density of states of disordered colloidal solids, *Science* **329**, 656-658 (2010).
- [21] Yethiraj, A. & Blaaderen, A. V. A colloidal model system with an interaction tunable from hard sphere to soft and dipolar. *Nature* **421**, 513-517 (2003).
- [22] Leunissen, M. E., *et al.* Ionic colloidal crystals of oppositely charged particles *Nature* **437**, 235-240 (2005).
- [23] For an N-particle system in 2D, there exist 2N normal modes. However, our measurements from 2000 frames can only yield 2000 modes (less than 2N). Therefore we renormalize  $D(\omega)$  correspondingly, by

requiring its integration over the 2000 modes equal to  $2000/2N$ . We also find that varying the number of frames can slightly change the shape of  $D(\omega)$  in the high-frequency regime ( $\omega > \omega^\ddagger$ ), but it has negligible effect on the low and medium frequency regimes ( $\omega < \omega^\ddagger$ ). Thus our main conclusions, mostly on the low and medium frequency regimes, are not affected.

- [24] Somfai, E. *et al*, Critical and noncritical jamming of frictional grains. *Phys. Rev. E* **75**, 020301(R) (2007).
- [25] Brito, C., & Wyart, M. Heterogeneous dynamics, marginal stability and soft modes in hard sphere glasses. *J. Stat. Mech.* **08**, L08003, (2007)
- [26] Widmer-Cooper, A., Perry, H., Harrowell, P. & Reichman, D. R. Irreversible reorganization in a supercooled liquid originates from localized soft modes. *Nat.Phys.* **4**, 711 (2008).
- [27] Brito, C., Dauchot, O., Biroli, G.& Bouchaud, J. Elementary excitation modes in a granular glass above jamming, *Soft Matter* **6**, 3013, (2010).
- [28] Shintani, H. & Tanaka, H. Frustration on the way to crystallization in glass. *Nat. Phys.* **2**, 200-206 (2006).
- [29] Watanabe, K. & Tanaka, H. Direct observation of medium-Range crystalline order in granular liquids near the glass transition. *Phys. Rev. Lett.* **100**, 158002 (2008).
- [30] Tanaka, H., Kawasaki, T., Shintani, H. & Watanabe, K. Critical-like behaviour of glass-forming liquids. *Nat. Mater.* **9**, 324-331 (2010).

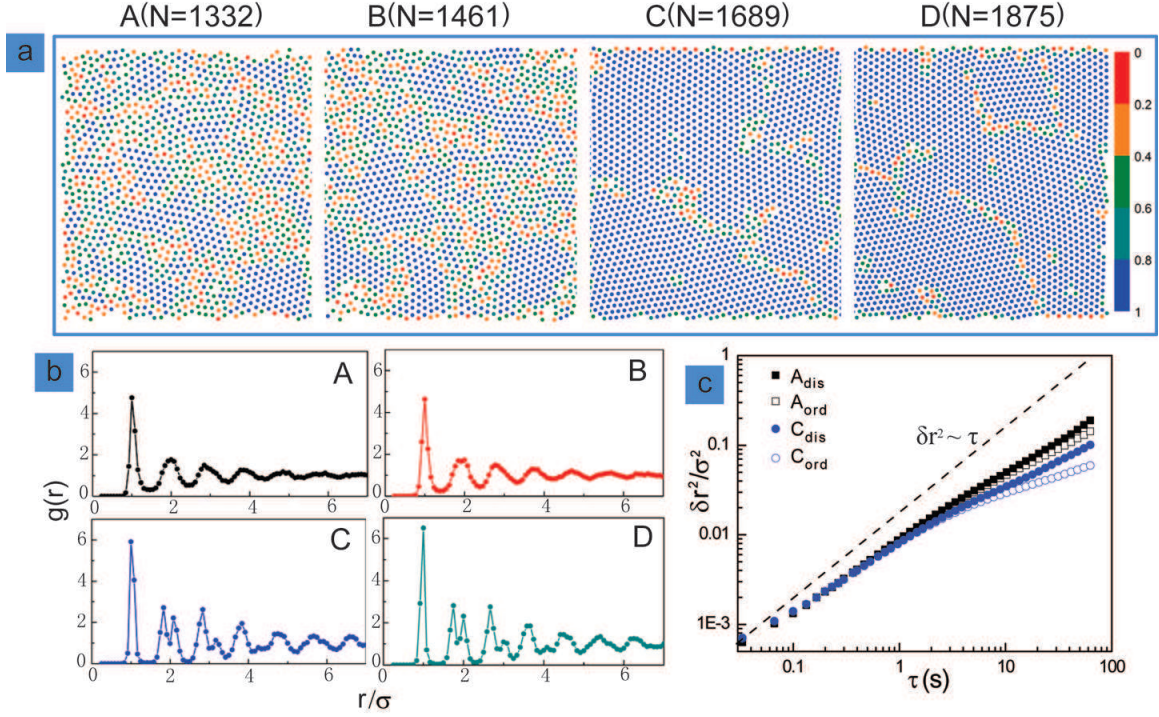


FIG. 1: **Structures and motions of four samples with different amount of disorder.** **a**, the structures by the particle equilibrium positions. The total dimensions are  $145 \times 145 \mu m^2$ . Different colors correspond to different  $\Psi_{6i}$  values. **b**, The pair correlation function,  $g(r)$ , of the four samples. The distance  $r$  is re-scaled by the position of the first-peak,  $\sigma$  ( $1.92a$ ,  $1.89a$ ,  $1.81a$  and  $1.73a$  from A to D). The peaks become more pronounced from A to D, indicating more order in the sample. **c**, MSD curves for the relatively disordered particles (solid symbols) and the relatively ordered particles (open symbols) in A and C. Higher MSD curves of the disordered particles demonstrate their larger motions. All curves are below the dashed line of free diffusion, as the result of caging effect.

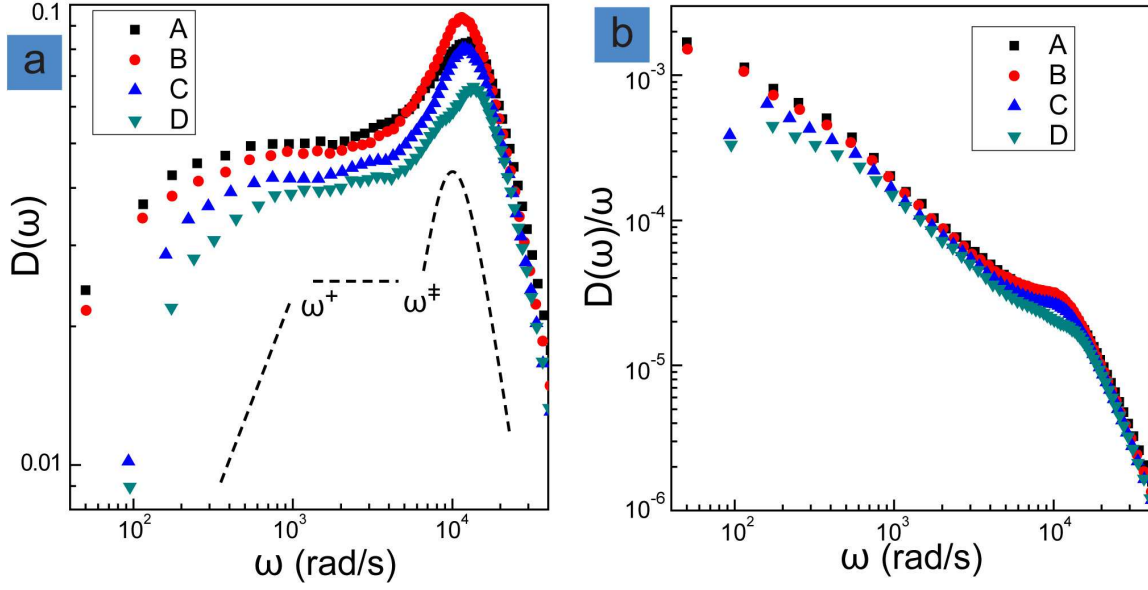


FIG. 2: **The distribution of the normal modes.** **a**, the density of states,  $D(\omega)$ , of the four samples. Each curve can be divided into three regimes by two characteristic frequencies,  $\omega^\dagger$  and  $\omega^\ddagger$ , as illustrated by the schematics. From A to D, as system disorder decreases, the number of the low-frequency modes reduces, the plateau width between  $\omega^\dagger$  and  $\omega^\ddagger$  shrinks, and the plateau height lowers. **b**, the  $D(\omega)/\omega^{d-1}$  spectrum. The Boson peak appears in C, D but shifts to lower frequencies in A, B. In both **a** and **b**, the highest frequency plotted is determined by our spatial resolution,  $15nm$ .

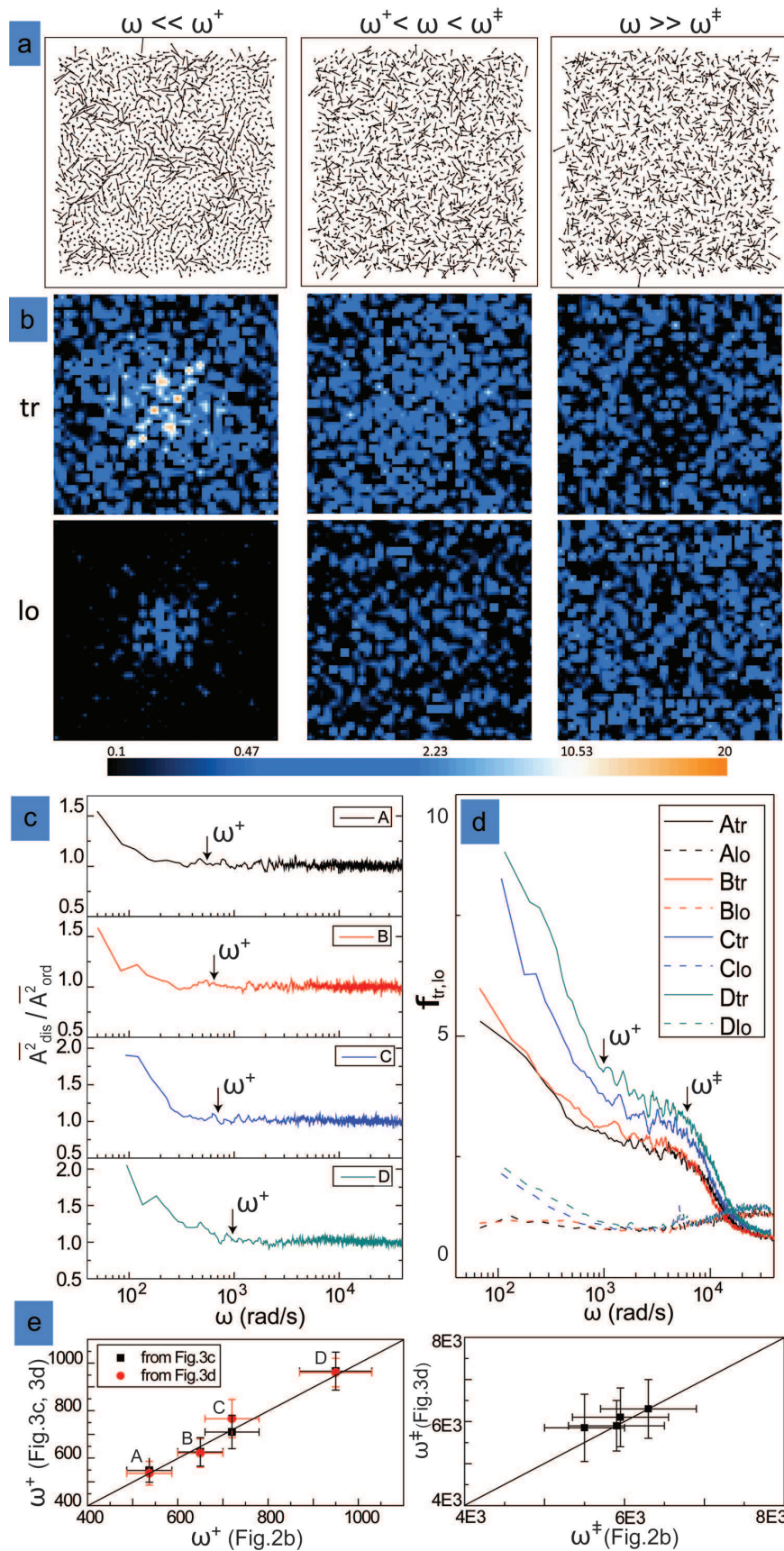


FIG. 3:  
12

**FIG. 3: Vibration distribution in real and Fourier space.** **a**, The polarization vectors of three typical modes in sample A. The three typical modes illustrate the properties of the three regimes. Clearly the low-frequency mode ( $\omega \ll \omega^\dagger$ ) has large-scale correlations, while the other two look rather random. **b**, The transverse and longitudinal components of the same modes in Fourier space. Both components are shown in the first Brillouin zone,  $[-\frac{\pi}{\sigma} < q_x, q_y < \frac{\pi}{\sigma}]$ . As  $\omega$  increases, the transverse component at small  $q$  varies from very large to very small values; while the longitudinal component keeps spreading throughout  $q$  space. **c**, the ratio of the mean squared vibration amplitude between the disordered particles and ordered particles,  $\overline{A^2}_{dis}/\overline{A^2}_{ord}$ . For small  $\omega$ , the ratio is larger than one, indicating stronger vibrations of the disordered particles. The transition frequency where it approaches unity defines  $\omega^\dagger$  separately. **d**, the average magnitude of transverse and longitudinal components at all frequencies. The average is taken over the small  $q$  area at the center,  $[-\frac{\pi}{2\sigma} < q_x, q_y < \frac{\pi}{2\sigma}]$ . The transverse curves (solid) dominate the longitudinal ones (dashed) mostly. We can again divide each transverse curve into three regimes, with two characteristic frequencies,  $\omega^\dagger$  and  $\omega^\ddagger$ . **e**, the comparison of  $\omega^\dagger$  and  $\omega^\ddagger$  determined by different approaches. They excellently collapse onto the straight line of  $y = x$ , confirming the robustness of the three regimes determined differently.

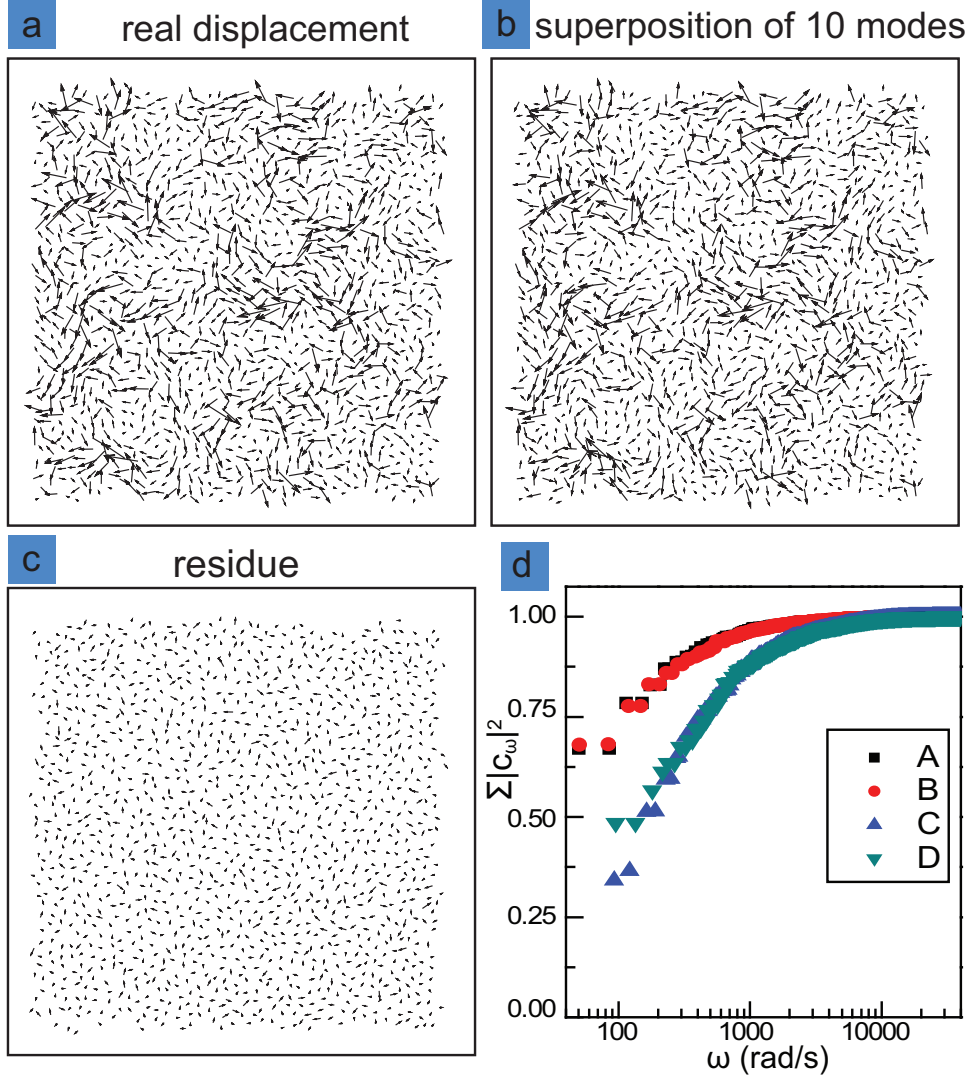


FIG. 4: **The comparison between the real dynamics and the superposition of low-frequency modes.** **a**, the displacement field during 2000 frames in sample A (enlarged 2.5 times for better illustration). **b**, the superposition of ten most contributed low-frequency modes. **c**, the residue from **a-b**. The small residue proves excellent agreement. **d**, the sum of the projection probabilities,  $|c_\omega|^2$ , for all the modes. Apparently the low-frequency modes make major contributions.